Clin Exp Metastasis (2008) 25:53–64
DOI 10.1007/s10585-007-9101-y

RESEARCH PAPER

A novel $\alpha_v\beta_3$-blocking disintegrin containing the RGD motive, Dis*Ba*-01, inhibits bFGF-induced angiogenesis and melanoma metastasis

Oscar H. P. Ramos · Alexandre Kauskot · Márcia R. Cominetti · Iga Bechyne · Carmen L. Salla Pontes · Fabrice Chareyre · Jan Manent · Roger Vassy · Marco Giovannini · Chantal Legrand · Heloisa S. Selistre-de-Araujo · Michel Crépin · Arnaud Bonnefoy

Received: 2 May 2007 / Accepted: 14 September 2007 / Published online: 19 October 2007

Abstract The integrin $\alpha_v\beta_3$ is involved in multiple aspects of malignant cancer, including tumor angiogenesis and metastasis, which makes the receptor a key target for the development of anti-cancer therapies. We report here on the production, the characterization and the in vivo anti-angiogenic and anti-metastatic properties of a novel $\alpha_v\beta_3$-binding disintegrin, Dis*Ba*-01, isolated from a cDNA library made with RNAs from the venom gland of *Bothrops alternatus*. The 11,637 Da-recombinant monomeric form of Dis*Ba*-01 displayed an RGD motif and interacted with purified $\alpha_v\beta_3$ integrin in surface plasmon resonance studies, in a dose-dependent and cation sensitive manner. A three-dimensional molecular model of Dis*Ba*-01 in complex with $\alpha_v\beta_3$ predicted a large surface of contacts with the β_3 subunit. Dis*Ba*-01 inhibited the adhesion of $\alpha_v\beta_3$-expressing human microvascular endothelial cell line-1 (HMEC-1) and murine melanoma cell line B16F10 to vitronectin (IC_{50} = 555 nM and 225 nM, respectively), and transiently inhibited their proliferation without direct cell toxicity, but did not affect the binding nor the proliferation of a human breast cancer-derived cell line (MDA-MB-231) not expressing $\alpha_v\beta_3$. In vivo, Dis*Ba*-01 dose-dependently decreased bFGF-induced angiogenesis in a matrigel plug assay in athymic nude mice (IC_{50} = 83 nM). When injected intravenously to C57BL/6 mice together with B16F10 melanoma cells, Dis*Ba*-01 time- and dose-dependently inhibited lung metastasis monitored by bioluminescent imaging. We conclude that Dis*Ba*-01 is a potent new inhibitor of $\alpha_v\beta_3$-dependent adherence mechanisms involved in neo-vascularization and tumor metastasis processes.

Keywords Disintegrin · $\alpha_v\beta_3$ · Angiogenesis · Metastasis · Bioluminescent imaging

Abbreviations

BFGF	Basic fibroblast growth factor
ECM	Extracellular matrix
FBS	Foetal bovine serum
FITC	Fluorescein isothiocyanate
GFP	Green fluorescent protein
HMEC-1	Human microvascular endothelial cell line-1

Oscar H. P. Ramos and Alexandre Kauskot contributed equally to this work.

O. H. P. Ramos · M. R. Cominetti · C. L. Salla Pontes · H. S. Selistre-de-Araujo
Dep. Ciências Fisiológicas, Universidade Federal de São Carlos, São Carlos, SP, Brasil

A. Kauskot · I. Bechyne · C. Legrand · M. Crépin · A. Bonnefoy
INSERM, U 553, Paris 75010, France

A. Kauskot · I. Bechyne · F. Chareyre · J. Manent · M. Giovannini · C. Legrand · A. Bonnefoy
Université Paris 7-Denis Diderot, Faculté de Médecine, IFR 105 -Saint Louis-Institut Universitaire d'Hématologie, Paris 75475, France

F. Chareyre · J. Manent · M. Giovannini
INSERM, U 674, Paris 75010, France

R. Vassy · M. Crépin
Laboratoire de Pharmacologie Clinique et Experimentale, Université Paris 13, CNRS UMR 7033, Bobigny 93000, France

A. Bonnefoy (✉)
Laboratoire d'Immunologie, Centre de Recherche du Centre Hospitalier de l'Université de Montréal-Saint-Luc, INSERM U743, 264, rue René Lévesque Est, Montreal, QC, Canada H2X1P1
e-mail: arnaudbonnefoy@yahoo.fr

IPTG	Isopropyl thio-β-D-galactopyranoside
MD	Molecular dynamics
MIDAS	Metal-ion-dependent adhesion site
MS	Mass spectroscopy
PCR	Polymerase chain reaction
PDB	Protein data base
RGD	Arginine-glycine-aspartic acid
RU	Resonance units
SVMP	Snake venom metalloproteinase
Vn	Vitronectin

Introduction

Tumorigenesis and metastasis processes involve sequential and inter-related mechanisms. These include tumor growth and tumor angiogenesis, detachment of tumor cells from the primary tumor, followed by migration through the local connective tissue and penetration into the circulation (intravasation). Once in the blood stream, tumor cells interact with circulating blood cells, arrest in the microvasculature of target organs, then extravasate and secondary proliferate. During each of these steps, integrin-mediated adhesion, migration, proliferation and survival of tumor cells and angiogenic endothelial cells play instrumental roles [1, 2].

The integrin $\alpha_v\beta_3$ is particularly important for tumor growth and invasiveness [3]. The receptor plays a major role in neo-vessels formation, its expression being strongly up-regulated in endothelial cells and specifically required during angiogenesis stimulated by basic fibroblast growth factor (bFGF) and tumor necrosis factor-α [4, 5]. $\alpha_v\beta_3$ is functionally involved in the malignant spread of various tumor cell types such as breast carcinoma, prostate carcinoma and melanoma, and supports tumor cell adhesion and migration through endothelium [6] and matrix proteins [1, 7].

Blocking $\alpha_v\beta_3$ is therefore expected to have a broad theoretical impact in cancer therapy and diagnosis. In the last decade, several clinical trials evaluating the efficacy of $\alpha_v\beta_3$ blockers have led to encouraging results. Thus, MEDI-522 (Vitaxin), a humanized antibody derived from the mouse LM609 monoclonal antibody, was recently reported to give positive results in a phase II trial enrolling patients with stage IV metastatic melanoma [8].

Some toxins from snake venom specifically and potently inhibit integrin functions. Among these, several disintegrins have demonstrated their anti-cancer properties. Albolabrin and contortostatin were reported to inhibit tumor metastasis by blocking tumor cell adhesion to ECM [9, 10]. Contortrostatin, salmosin, accutin or rhodostomin were described with anti-angiogenic and anti-metastatic activities [11–15]. Disintegrins are a family of non-enzymatic, low-molecular-weight, cystein-rich peptides usually derived from proteolytic processing of Snake Venom Metalloproteinases (SVMPs). SVMPs are multi-domain zinc-dependent proteinases classified into four types (P-I, P-II, P-III, P-IV) according to their domains composition. P-I SVMPs are composed of a peptide signal, a pro-domain and a metalloproteinase domain; P-II class has a metalloproteinase and a disintegrin-like domain. The P-III class contains a cystein-rich domain in addition to the metalloproteinase and the disintegrin-like domain, whereas P-IV SVMPs comprise an additional lectin-like domain [16]. Most of the P-II SVMPs-derived disintegrins contain the RGD or the KGD sequence which acts as a potent antagonist of β_1 and β_3 integrins, in particular, $\alpha_5\beta_1$, $\alpha_{IIb}\beta_3$ and $\alpha_v\beta_3$ [17].

In the present work, we report on the identification, the production and the functional characterization of a novel P-II SVMP-derived RGD-disintegrin produced by recombinant DNA techniques from the venom gland RNAs of *Bothrops alternatus* (urutu) snake. (Dis*Ba*-01, Genbank accession no. **AY259516**). We show that Dis*Ba*-01 interacts with $\alpha_v\beta_3$ integrin and demonstrate its anti-adhesive properties in vitro, and its potent anti-angiogenic and anti-metastatic activities in murine models.

Material and methods

Dis*Ba*-01 PCR cloning

Total RNA was isolated from the venom glands of a *Bothrops alternatus* specimen with Trizol (Invitrogen—Carlsbad, CA, USA) and the mRNA fraction was purified using the PolyAtract system (Promega, Pittsburgh, PA, USA). A cDNA library was made using UNIZAP system (Stratagene, La Jolla, CA, USA) and used as template for PCR amplification. PCR primers were designed based on disintegrin DNA sequences from snake venoms and were used as an attempt to amplify homologous disintegrins from *Bothrops alternatus*. To facilitate the DNA cloning, *Bam* HI and *Eco* RI restriction sites were added, respectively, to the forward primer (5′-CGC-GGATCC-GGAAATGAACTTTTGGAG-3′) and the reverse primer (5′-TCC-GAATTC-TCAAATCTGAGAGAAG-3′). The PCR product and pET28a vector (Novagen—Madison, WI, USA) were digested with the same restriction enzymes, purified from 1% agarose gels and ligated using T4 DNA ligase (Invitrogen—Carlsbad, CA, USA). After the transformation of the *Escherichia coli* DH5-α cells, the kanamycin-resistent recombinant plasmids were selected for restriction analysis and the positive clones were automatically sequenced in an ABI Prism 377 DNA Sequencer (Perkin Elmer—Foster City CA, USA). The confirmed

recombinant plasmids (pDis*Ba*-01) were used to transform *Escherichia coli* BL21(DE3) strain.

Expression and solubility

Cultures of *Escherichia coli* BL21(DE3) pDis*Ba*-01 cells were induced by 0.5 mM isopropyl thio-β-D-galactopyranoside (IPTG) addition. Three hours after the induction, the cells were harvested by centrifugation (4,200*g*; 15 min), suspended in buffer A (40 mM Tris–HCl, pH 7.9, 0.5 M NaCl and 5 mM imidazol) and lysed by sonication (6 times, 4°C, 10 s interval). The soluble cellular fraction (S1) was obtained by centrifugation (27,500*g*; 15 min) and the sediment was suspended in buffer A containing 6 M urea (buffer B), sonicated 6 times (4°C, 10 s interval) and incubated in ice bath for one hour. The soluble fraction obtained in denaturing condition (S2) was separated by centrifugation (27,500*g*; 15 min). The samples were analyzed by SDS-PAGE.

Protein purification

The His-Tag fused target protein was purified by a two-step process. First, affinity chromatography (Ni-NTA Sepharose, Qiagen) was performed under denaturing conditions at room temperature. The column was equilibrated with buffer B and the sample was applied. After washing out unbound proteins, the target protein was eluted with an isocratic gradient with 4 column volumes of buffer C (40 mM Tris–HCl, pH 7.9, 0.5 M NaCl, 20 mM imidazol and 6 M urea) and 4 column volumes of buffer D (40 mM Tris–HCl, pH 7.9, 0.5 M NaCl, 1 M imidazole and 6 M urea). The fractions were analyzed by SDS-PAGE and the protein of interest was dialyzed once against 25 volumes of 3 M urea in water and then 3 times against 50 volumes of water at 4°C to completely remove the denaturing agent. The sample was loaded onto a Mono Q 5/50 column (GE Healthcare) and separated in a constant flow (1.0 ml/min) with a NaCl linear gradient (0–1 M) with 20 mM Tris–HCl, pH 8.6 buffer. Fractions with the expected size in 15% SDS-PAGE gels were pooled, dialyzed three times against 50 volumes of water at 4°C and kept at –20°C until use. Protein concentration was estimated by the Bradford method.

Protein characterization

N-terminal analysis of the purified protein was performed by Edman degradation on a Shimadzu PPSQ-20. The resulting amino acid sequence was compared to the predicted one from DNA sequence using MULTALIN. The molecular mass of the purified protein was determined by mass spectrometry (MS). The sample was desalted in a resin R2 PORES, activated with methanol, equilibrated with 0.2% formic acid and eluted in 30 µl of 0.2% formic acid in 50% of acetonitrile just before the MS analysis (Quattro II, Micromass, Manchester, UK). The mass spectra in MS1 were collected during 2 min with 2.75 s/scan (total of 43 scans). The resultant spectrum was convoluted to molecular mass with the MaxEnt1 program (MassLynx v.3.3).

In silico studies of Dis*Ba*-01 and its complex with $\alpha_v\beta_3$ integrin

The disintegrin model was generated using homology modeling by satisfaction of spatial restraints implemented in Modeller 8v2 [18]. The templates were the crystal structure of trimestatin [19] (Genbank accession no. **37926519**; PDB: 1J2L; 75,65% of identity) and the solution structure of flavoridin [20] (Genbank accession no. **AB052155**; PDB: 1FVL; 74,65% of identity). The model with the best variable target function was chosen from 100 initial models and analyzed by Procheck [21], Verify 3D [22] and the module Qualty of WhatIf [23] to search for problematic regions.

Various studies have indicated that the aspartic acid present at the RGD sequence should be involved in interactions with a metal coordinated at metal-ion-dependent adhesion site (MIDAS) of β subunits [24–26]. Thus, we superposed the RGD motif of Dis*Ba*-01 to the same sequence found in a peptide complexed to $\alpha_v\beta_3$ integrin (PDB: 1L5G [25]), removed the peptide and replaced the original manganese atoms by calcium atoms. The whole model was subject to energy minimization (EM) and short time-scale molecular dynamics (MD) in water to relax the structure of the complex. The EM was based on 1 step of steepest descent each 100 steps of conjugate gradients and the MD was conducted during 10.0 ps (using temperature and pressure coupling) in water containing ions (Na^+ and Cl^-) in a concentration that at the same time simulate physiological solutions and neutralizes the system. Both calculations were executed using algorithms found in GROMACS package [27]. The interface area of the final complex model was determined by subtracting the complex area from the sum of the free molecule areas using Surface Racer [28].

Biospecific interaction analysis (BIA)

Binding of Dis*Ba*-01 (incrementing concentrations from 0.06 µM to 19 µM) to immobilized $\alpha_v\beta_3$ integrin was done via surface plasmon resonance, using a BIAcore 2000 system

(BIAcore, Uppsala, Sweden). The purified $\alpha_v\beta_3$ integrin (25 μg/ml in 10 mM sodium acetate, pH 5.0) was covalently attached via amine coupling to sensor chip CM5, according to the instructions of the manufacturer, to 3,700–9,500 resonance units (RU). Bound ligand was then perfused in 10 mM HEPES, 150 mM NaCl, 0.005% Surfactant P20, pH 7.4 at 25°C at a flow rate of 30 μl/min. The specificity of analyte binding was analyzed by correction for non-specific binding, *via* perfusion of non-coupled control channels. Association and dissociation rate constants were calculated via curve fitting, using the BIAevaluation software (version 4.1), assuming a 1:1 model, considering Dis*Ba*-01 as monomeric with a M_r 11,780. The rapid increase and decrease in resonance signal, preceding association and dissociation respectively (buffer jumps), were excluded from evaluation. The chip was regenerated by injection of GlyHCl 3 M without or with EDTA 30 mM for 10 s.

Cell lines and culture

B16F10 (LGC Promochem) murine melanoma cells were grown in Dulbecco's modified Eagle's medium (DMEM, Invitrogen) containing 10% (v/v) fetal bovine serum (FCS) and 60% (v/v) NaCl (150 mM). The luciferase- and GFP-expressing B16F10-derived 2B8 cell clone was obtained by transfection of B16F10 cells with pEGFPLuc (BD Biosciences, Rungis, France), a plasmid that contains the genes for neomicine resistance, GFP and luciferase expression. Cells, between the 27th and 32th passage were cultured in DMEM containing 10% FBS (v/v) and 30% (v/v) NaCl (150 mM), supplemented with 0.8 mg/ml G418 (Invitrogen). MDA-MB-231 (ATCC) cell line from estrogen-independent mammary carcinoma was cultured between the 90th and 100th passage in DMEM containing 10% FBS (v/v), 15 mM HEPES and 5 μg/ml fungizone. This cell clone cultured at particularly late passage was chosen for its low expression level of $\alpha_v\beta_3$ (see Fig. 5). Human microvascular endothelial cells (HMEC-1), a kind gift of Drs E.W. Ades and T.J. Lawley (Centers for Disease Control and Prevention and Emory University School of Medicine, Atlanta, GA), between the 10th and 16th passage, were cultured in MCDB-131 (Invitrogen) supplemented with 10% FBS (v/v), 10 ng/ml EGF and 1 μg/μl hydrocortisone. All cell lines were cultured in the presence of penicillin (100 UI/ml), streptomycin (100 μg/ml) and L-glutamine (2 mM), in a humidified environment with 5% CO_2 at 37°C.

Cell adhesion and proliferation assays

B16F10, HMEC-1 or MDA-MB-231 cells, detached from culture dishes with 0.53 mM EDTA, were resuspended in PBS containing 0.9 mM calcium and 0.5 mM magnesium, centrifuged at 290*g* for 5 min, resuspended in DPBS. Cells were pre-incubated at 37°C for 30 min with 0–1,000 nM of Dis*Ba*-01 and seeded (5×10^4 cells per well) for 1 h at 37°C in 96 well plates pre-coated with 1 μg/ml vitronectin (Promega). After washing with PBS, adhered cells were stained by incubation with 0.5% crystal violet in 20% methanol (50 μl/well) for 1 h at room temperature followed by extensive washing. Wells were then incubated for 30 min at room temperature with a solution of ethanol:citrate 0.1 M (1:1) pH 4.2 and read at 540 nm in an ELISA reader (Labsystems). To assess the effect of Dis*Ba*-01 on cell proliferation, HMEC-1, B16F10 or MDA-MB-231 were seeded in 96 well plates (2×10^4 cells/well) in the same mediums used for their culture (200 μl) and let to adhere for 7 h. Increasing concentrations of Dis*Ba*-01 (0–100 nM) were then added, for additional 24, 48 or 72 h of incubation. Cells were then washed twice with PBS, incubated for 4 h at 37°C with medium containing XTT reagent (Cell Proliferation kit II, Roche) and plates were read according to the manufacturer's instructions.

Effects of Dis*Ba*-01 on in vivo angiogenesis in matrigel

Experimental procedures performed on animals were done according to the French legislation on protection of animals. The effect of Dis*Ba*-01 on angiogenesis was investigated by a Matrigel plug assay [29]. Briefly, samples of Matrigel (9.2 mg/ml; Becton Dickinson) in liquid form at 4°C were supplemented with 1 μg bFGF plus Dis*Ba*-01 (0–1000 nM). The mixtures (300 μl) were injected into the abdominal subcutaneous tissue of nude mice. After 14 days, the mice were killed and Matrigel plugs were removed and fixed with paraformaldehyde (4%) until analysis. After embedded in paraffin, Matrigel plugs were sectioned at 4 μm and stained with Masson-Trichrome. For angiogenesis quantification, stained endothelial cells and functional capillaries containing red blood cells were counted.

Effects of Dis*Ba*-01 in a bioluminescent model of lung melanoma metastasis

The anti-metastatic activity of Dis*Ba*-01 was evaluated by injecting the luciferase-expressing B16F10-2B8 clone in C57BL6/j mice (8–10 weeks old). Briefly, 5×10^5 cells pre-incubated for 5 min with increasing concentrations of Dis*Ba*-01 (0, 0.05, 0.5, 2 or 4 mg/kg) were injected (100 μl) in the tail vein. The progression of pulmonary metastases was measured at day 1, 4, 7, 11 and 14 following cell inoculation by an imaging system (IVIS™

100 Xenogen, Alameda, USA). For this purpose, mice were shaved on surfaces of interest to maximize the photon emission. After intra-peritoneal injection of D-luciferin (150 mg/kg)—which cleavage by luciferase produces visible light—mice were anesthetized with 2.5% isoflurane, and placed onto the warmed stage in the imaging chamber during a 5 min-continuous exposure in ventral views. Light emission on displayed images was quantified as total photons per second using *Living Image software*. At day 14, a group of mice was injected with 1 mg/kg of Dis*Ba*-01 repeated 3 days later, in order to analyze the reversal of tumoral foci already installed.

For ex vivo imaging, mice received 150 mg/kg D-luciferin i.p., 5 min before euthanasia and necropsy. Lungs were excised, placed individually into 24-well tissue culture plates with 300 µg/ml D-luciferin in DPBS, and imaged for 30 s. The surface of the lungs covered by pigmented nodules was quantified in parallel, using the *ImageJ 1.34s N.I.H.* software. For histological observations, tissues were embedded in paraffin and 5 µm-sections were hydrated and stained with Hematoxylin-Eosin.

Results

Identification and production of recombinant Dis*Ba*-01

*Dis*Ba-*01 cloning*

A band of 339 bp was amplified from the cDNA library using primers specific for snake venom disintegrins. The PCR product and pET28a were restricted and ligated. The recombinant vector (pDis*Ba*-01) was used in the transformation of *Escherichia coli* DH5-α cells. The success of the cloning process was confirmed by restriction analysis and sequencing (Fig. 1a). No frame shift was detected in the cloning and the insert revealed to be a coding region corresponding to a medium disintegrin (78 amino acids, ~8 kDa) with an RGD adhesive motif (amino acids 56–58). The fusion protein produced in *E. coli* pDis*Ba*-01 is a 11,780 kDa protein as expected and estimated by SDS-PAGE. Dis*Ba*-01 shows remarkable sequence similarities with a variety of members of the disintegrin family (Fig. 1b).

Protein expression, purification and characterization

Escherichia coli BL21(DE3) cells were transformed by pDis*Ba*-01 and the expression of Dis*Ba*-01 was investigated by SDS-PAGE analysis. We observed the expression of a low molecular weight protein after the IPTG induction (Fig. 2a). The target protein was expressed as inclusion bodies, but could be recovered in denaturing conditions using 6 M urea. The proteins from bacterial extract solubilized in denaturing buffer A were submitted to a metal chelating affinity chromatography using Ni-NTA resin. The target protein, Dis*Ba*-01, bound to the resin and was eluted, together with some contaminant proteins (Mr between 20 kDa and 30 kDa), with isocratic gradient denaturing buffer containing imidazole. The eluate was further resolved into three major peaks by anion exchange chromatography (Fig. 2b). The analysis of the second peak revealed that Dis*Ba*-01 could be purified to homogeneity (Fig. 2a, lane D). Dis*Ba*-01 was identified by N-terminal sequencing of its first 20 residues (Fig. 2c). The amino acid sequence had 100% identity with the predicted sequence for the fusion protein. The recombinant protein was ionized and the mass spectrum was determined as 11,637 Da (Fig. 2d).

In silico studies

A molecular model of Dis*Ba*-01 was constructed by homology modeling and submitted to quality evaluation software. No residue was found outside the most favorable region and additional allowed regions of the Ramachandran plot. Further analysis of the main-chain and side-chain stereochemistry, atomic contacts and chemical environment also revealed that the model values perfectly fit the expected values. The predicted structure exhibits characteristics that resemble its major template, trimestatin, including 6 disulfide bonds, an elongated shape, and regions of similar electrostatic potential. Their root mean square deviation (RMSD) for backbone atoms superposition was 0.59 Å. Despite the high similarity between template and model, some differences could be noticed such as the conformation of the RGD motif and the fact that Dis*Ba*-01 has a bigger area of negative electrostatic potential (Fig. 3a).

To investigate structural features of the binding of Dis*Ba*-01 to the integrin $\alpha_v\beta_3$, the RGD motif from the model of Dis*Ba*-01 was superimposed to the structure of a RGD peptide complexed with $\alpha_v\beta_3$. After EM and short time-scale MD (10 ps) the model was subjected to analysis (Fig. 3b, c). The aspartic acid D58, comprised in the RGD motif, was found to interact with metal ion coordinated at MIDAS of β_3 subunit. The distances observed for its carbonyl oxygen atoms, O delta 1 and O delta 2, to the metal were 2.61 and 2.51 Å, respectively. Three residues downstream the RGD motif, the D61 points directly to the calcium atom coordinated at ADMIDAS (adjacent to MIDAS). In the opposite side of the disintegrin molecule, a positive surface cluster comprising the side-chains of residues R53, R56 (comprised in the RGD motif) and R73

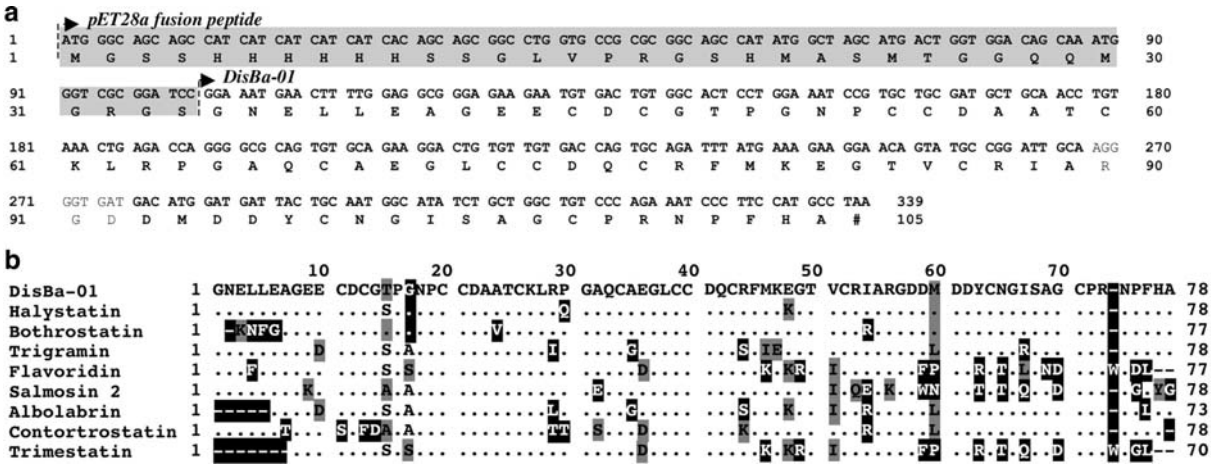

Fig. 1 (**a**) Nucleotide and deduced amino acid sequences from pDis*Ba*-01. The fusion peptide from the pET28a vector is shown in gray background. The RGD motif is shown in gray and the stop codon is represented by "#". (**b**) Comparison of Dis*Ba*-01 sequence with other members of disintegrin family. The multiple alignment includes Halystatin (gi: **469190**), Bothrostatin (gi: **13194760**), Trigramin (gi: **86026**), Flavoridin (gi: **21326758**), Salmosin 2 (gi: **3643793**), Albolabrin (gi: **104446**), Contortrostatin (gi: **48428162**) and Trimestatin (gi: **37926519**). Residues identical to Dis*Ba*-01 are represented by dots, conserved residues are shown in white background. Similar but non-conserved residues are shown in gray background and substitutions for non-similar residues are shown in black background

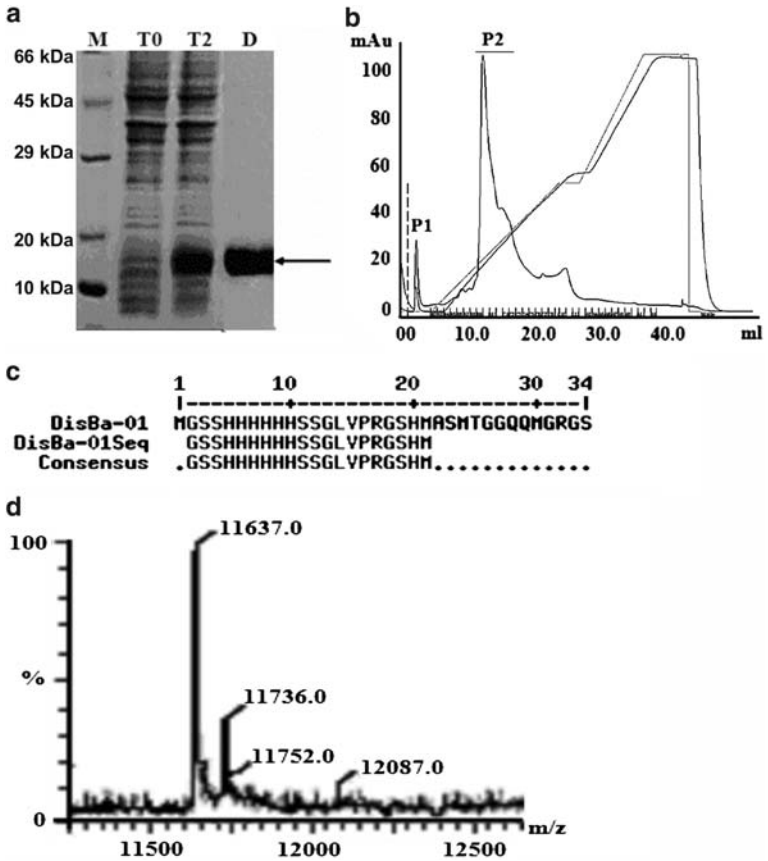

Fig. 2 *Expression, purification and characterization of recombinant* Dis*Ba*-01. (**a**) The recombinant protein was expressed by *E. coli* BL21(DE3) fused to pET28a His-Tag. (M): molecular mass marker; (T0): culture sample before IPTG induction, (T3): culture sample 3 h after IPTG induction; (D): recombinant Dis*Ba*-01 after purification by anion exchange chromatography. (**b**) Anion-exchange chromatography profile. (**c**) N-terminal amino acid sequence of the recombinant Dis*Ba*-01 was determined by Edman degradation and compared with the predicted sequence for the sequencing of the expression vector. (**d**) Mass spectrum of ionized Dis*Ba*-01

points to negative regions of α_v subunit including residues D150, D218. Furthermore, R56 forms a hydrogen bridge with the oxygen atom of the main-chain of A149 (α_v subunit). Also the last C-terminal residues of Dis*Ba*-01 exhibit several interactions. H77 is involved in hydrogen bridge with D148 (α_v subunit) and hydrophobic contacts with Y166 (β_3 subunit). F76 is involved in hydrophobic interactions with R214 and R216 of the β_3 subunit. The

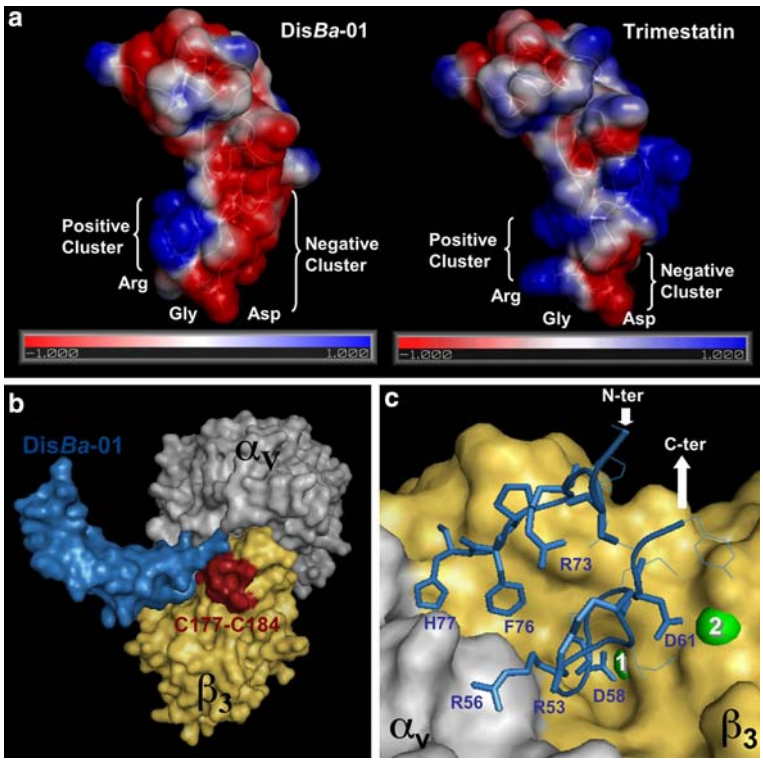

Fig. 3 (**a**) Electrostatic potential of Dis*Ba*-01 (Left) and Trimestatin (right). The calculations were made using APBS [33]. The residues that constitute the RGD motif are indicated by the 3-letter code. Dark blue surface represents positive electrostatic potential, while red surface indicates negative electrostatic potential. (**b**) The general aspect of the α_V chain (grey), the β_3 chain (yellow) and Dis*Ba*-01 (blue) in the predicted $\alpha_v\beta_3$-Dis*Ba*-01 complex is represented as molecular surface colored by chains. The residues C177-C184 (sequence CYDMKTTC), part of the epitope of the LM609 antibody on the β_3 subunit [30] are coloured in dark red. (**c**) Zoom to the interface region between Di*Ba*-01 (blue sticks), integrin α_V (grey) and β_3 yellow chains represented by their molecular surfaces. Dis*Ba*-01 key contact residues are indicated by 1 letter code plus the residue number. Calcium atoms are represented by spheres and are colored in green. Calcium 1 corresponds to the metal coordinates at MIDAS and calcium 2 to the metal coordinated at ADMIDAS

interface of the complex covers 696.38 Å^2, about 16% of the disintegrin's molecular surface area (MSA). The C177-C184 residues, required for the recognition of the β_3 subunit by the LM609 Monoclonal antibody [30], are close to and partly overlapping with the surface covered by the disintegrin (Fig. 3b). When comparing the free and bound predicted forms of Dis*Ba*-01 it is possible to note great flexibility, even in this short simulation. Main-chain conformational shifts were mainly visible in the loop that contains the RGD motif and the C-terminus of the molecule, regions of the disintegrin that interacts with the integrin. For the RGD plus 2 residues at each side of this motif (7 residues), the root mean square (RMS) of all atoms was 1.36 Å (0.74 Å for backbone only) and for the NPFHA C-terminal sequence it was 1.26 Å (0.99 Å for backbone only).

Dis*Ba*-01 binds to the integrin $\alpha_v\beta_3$

Surface plasmon resonance analyses confirmed that the recombinant Dis*Ba*-01 injected at increasing concentrations specifically interacted with the purified integrin $\alpha_v\beta_3$ immobilized onto the sensor chip (Fig. 4a). Non-specific binding was estimated by applying bovine serum albumin (BSA). The complex dissociation was slow and allowed to calculate a K_d of 1.76×10^{-3} 1/second and a K_D of 1.6×10^{-7} M. The regeneration of $\alpha_v\beta_3$ immobilized on the sensor chip could be achieved by perfusing GlyHCL pH 3 during 30 s. The procedure led to partial lost of integrin on the surface of the chip, visualized by a drop in the RU signal, but allowed de novo binding of Dis*Ba*-01. In contrast, perfusion of GlyHCL pH 3 supplemented with EDTA 30 mM almost abrogated subsequent binding of the disintegrin, although stable residual binding was readily measured (Fig. 4b).

Dis*Ba*-01 inhibits cell adhesion and proliferation to Vitronectin

Dis*Ba*-01 dose-dependently inhibited the adhesion of B16F10 and of HMEC-1 to Vn, with IC_{50} of 225 nM and 555 nM, respectively (Fig. 5a). By contrast, Dis*Ba*-01

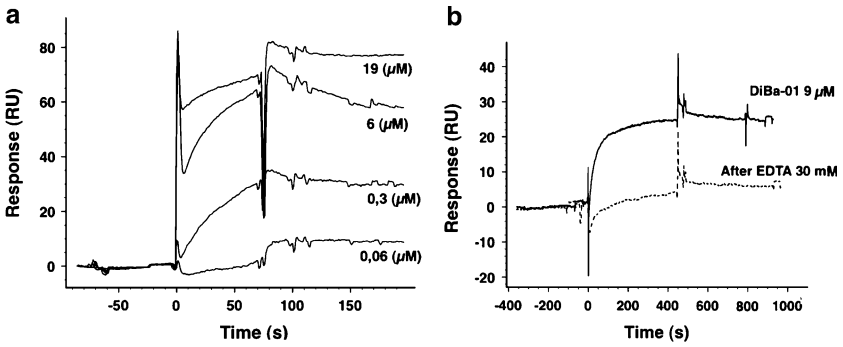

Fig. 4 *Biospecific interaction analysis of* Dis*Ba*-01 *with* $\alpha_v\beta_3$ *integrin*. (**a**) Representative tracings of association and dissociation of the indicated concentrations of Dis*Ba*-01, during perfusion at 30 μl/min over dextran-insolubilized $\alpha_v\beta_3$ integrin. (**b**) Effect of the pre-injection of GlyHCl 3 M without or with EDTA 30 mM for 10 s on the interaction of Dis*Ba*-01 (9 μM) with $\alpha_v\beta_3$ immobilized on the sensor chip

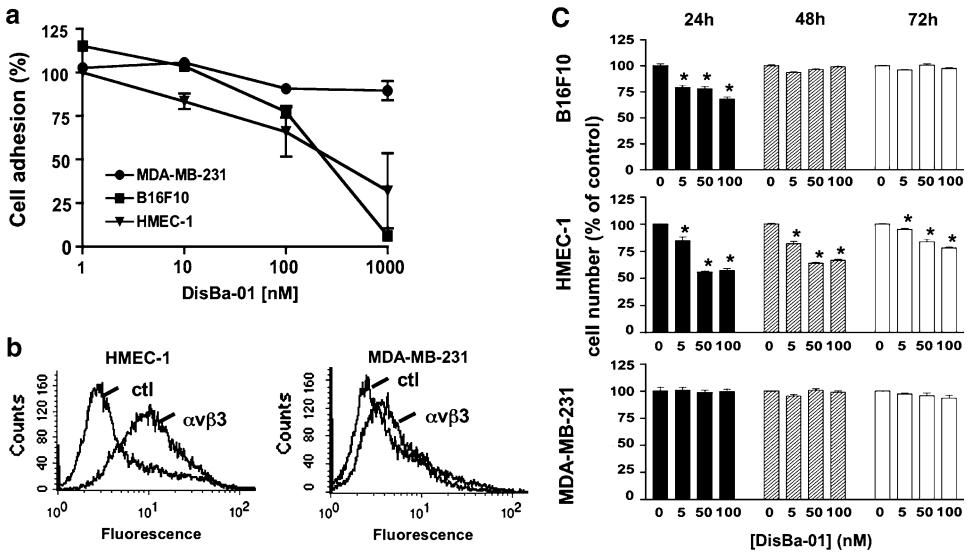

Fig. 5 *Inhibition of the adhesion of B16F10 and HMEC-1 cells but not MDA-MB-231 cells on vitronectin by* Dis*Ba*-01. (**a**) B16F10, HMEC-1 and MDA-MB-231 cells were seeded in 96-well plates in the presence of increasing concentrations of Dis*Ba*-01 (0–1000 nM). Cell adhesion was measured by crystal violet staining. (**b**) Surface expression of $\alpha_v\beta_3$ on HMEC-1 and MDA-MB-231 cells was detected by flow cytometry using the LM609 antibody. (**c**) Inhibition of the proliferation of B16F10 and HMEC-1 cells but not MDA-MB-231 cells on vitronectin by DisBa-01. B16F10, HMEC-1 and MDA-MB-231 proliferation on immobilized Vn was measured at 24 h, 48 h or 72 h in the presence of increasing concentrations of Dis*Ba*-01 (0–100 nM) using an XTT assay as described in the Methods. Results are expressed as percentages of control value without Dis*Ba*-01 (mean ± SEM of triplicate experiments). Asterisk indicates a P value < 0.01 determined using a Mann–Whitney test

failed to significantly inhibit the adhesion to Vn of the human breast cancer cell line, MDA-MB-231. The B16F10 melanoma cell line was reported to express high levels of $\alpha_v\beta_3$ [31]. HMEC-1 cells, but not MDA-MB-231, expressed $\alpha_v\beta_3$ on their surface, as detected by flow cytometry (Fig. 5b). Dis*Ba*-01 dose-dependently impaired the proliferation of B16F10 and HMEC-1—the effect being significant at 24 h for B16F10 (up to 35% inhibition) (Fig. 5c) and at 24, 48 and 72 h for HMEC-1 (up to 42% of inhibition after 24 h)—but had no significant effect on MDA-MB-231 proliferation, even at the highest dose (100 nM) (Fig. 5c). Additional assays using XTT reagent revealed no cytotoxicity of Dis*Ba*-01 when incubated with B16F10 or HMEC-1 cells in culture in 96 well-plates at doses up to 50.9 μM (not shown). Apoptosis assays using an annexin V-FITC kit performed on HMEC-1 in suspension revealed no pro-apoptotic activity of Dis*Ba*-01 at 1 μM (not shown).

Dis*Ba*-01 suppresses in vivo angiogenesis

$\alpha_v\beta_3$-dependent adhesive functions of endothelial cells are essential for the formation of neo-vessels. We therefore

tested the capacity of Dis*Ba*-01 to inhibit angiogenesis induced by bFGF, in a Matrigel plug injected sub-cutaneously in athymic nude mice [29]. Dis*Ba*-01 was incorporated in the Matrigel at various concentrations and angiogenesis progression was evaluated after 14 days by histological staining. Endothelial cell number was significantly and dose-dependently decreased by up to 61 ± 3.3% (SEM) at 1000 nM of Dis*Ba*-01 (Fig. 6a), the disintegrin being effective at a concentration of 20 nM (23.2 ± 3.4% of inhibition; SEM). The number of neo-vessels formed was also drastically reduced, down to 7.7 ± 2.2% (SEM) of the control value at 1000 nM (IC_{50} = 83 nM) (Fig. 6b).

Dis*Ba*-01 inhibits pulmonary melanoma metastasis

To evaluate the capability of Dis*Ba*-01 to prevent metastasis we used a mouse model of lung colonization by a B16F10 melanoma sub-clone (B16F10-2B8) transfected with the luciferase gene, allowing non-invasive bioluminescent imaging (BLI). Transfected B16F10-2B8 cells were selected for their in vitro and in vivo phenotype—morphological aspect and growth rate—comparable to the parental B16F10, and for their stable luciferase activity measured in vitro and in vivo (unpublished data). B16F10-2B8 (5×10^5 cells) were co-injected with various concentrations of Dis*Ba*-01 (0.05 to 4 mg/kg) in the tail vein of C57BL/6j syngeneic mice and the luciferase activity of proliferative melanoma cells localized in the lungs was measured during 14 days. Figure 7a shows that Dis*Ba*-01 time- and dose-dependently suppressed the bioluminescent signal (photons per second) arising from the lungs, the anti-metastatic effect being close to the maximal at 2 mg/kg, with 69.8 ± 11.7% of inhibition at day 14 (Fig. 7b). Ex vivo analyzes performed at day 14 confirmed the protective effect of the disintegrin. Excised lungs of mice treated with a bolus of 2 mg/kg of Dis*Ba*-01 showed a reduction of 72.8 ± 8.0% of the surface covered by pigment melanoma foci (Fig. 7c), very comparable to in vivo BLI measurements. Further histological analyses of lung cross-sections stained with hematoxylin-eosin dye also confirmed a reduction of the number of micrometastases formed within the pulmonary tissue of mice treated with Dis*Ba*-01 (2 mg/kg) (Fig. 7d). In additional experiments, we tested the ability of Dis*Ba*-01 to resorb pre-existing lung metastasis. Dis*Ba*-01 (1 mg/kg) injected i.p. at day 14 and 17 following B16F10-2B8 cell inoculation failed to reduce the exponentially increasing bioluminescent signal (measured up to day 21) produced by metabolically active melanoma cells (not shown).

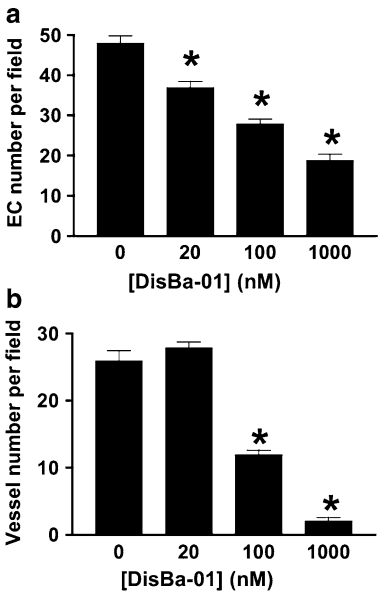

Fig. 6 *Inhibition of bFGF-induced angiogenesis "in vivo" by* Dis*Ba*-01. The formation of neo-vessels in a Matrigel plug containing bFGF injected sub-cutaneously in athymic nude mice (3 mice per group) was quantified in the presence of increasing concentrations of Dis*Ba*-01 (0–1000 nM). Fourteen days after their injection, Matrigel plugs were harvested and processed for histological analysis. The number of stained endothelial cells (EC) (**a**) and capillaries containing red blood cells (**b**) were measured for each condition in Matrigel sections (three Matrigels per point and at least 6 slides per Matrigel). Results are expressed as mean ± SEM. Asterisk indicates a P value <0.001 determined using a Mann–Whitney test

Discussion

The analysis of the electrostatic potential of Dis*Ba*-01 revealed a bi-polarity of the molecule comprising regions adjacent to the R56 (positive potential) and D58 (negative potential). In disintegrin molecules, R56 is frequently associated with other positively charged residues, forming a positive cluster. This feature was also found in trimestatin and flavoridin, suggesting relevance for this region during the docking to α subunits that are recognized by these toxins [19]. Comparing the free and $\alpha_v\beta_3$-complexed Dis*Ba*-01 models, it was possible to observe structure flexibility in the RGD loop and the C-terminus, in agreement with previous studies [32]. In our model, the N-terminus of the disintegrin seems not to make any important interaction with the integrin subunits and most of the contacts observed engage the β_3 subunit. In support to this model, we found that chinese hamster ovary (CHO) cells transfected with the β_3 subunit are more prone to adhere to immobilized Dis*Ba*-01 than untransfected CHO cells (personal results). Dis*Ba*-01 was found to interact with the purified $\alpha_v\beta_3$ in surface plasmon resonance studies in a specific and stable manner (K_D: 1.6×10^{-7} M). This interaction was inhibited by EDTA, indicative for a cation-sensitive binding as also reported for other disintegrins

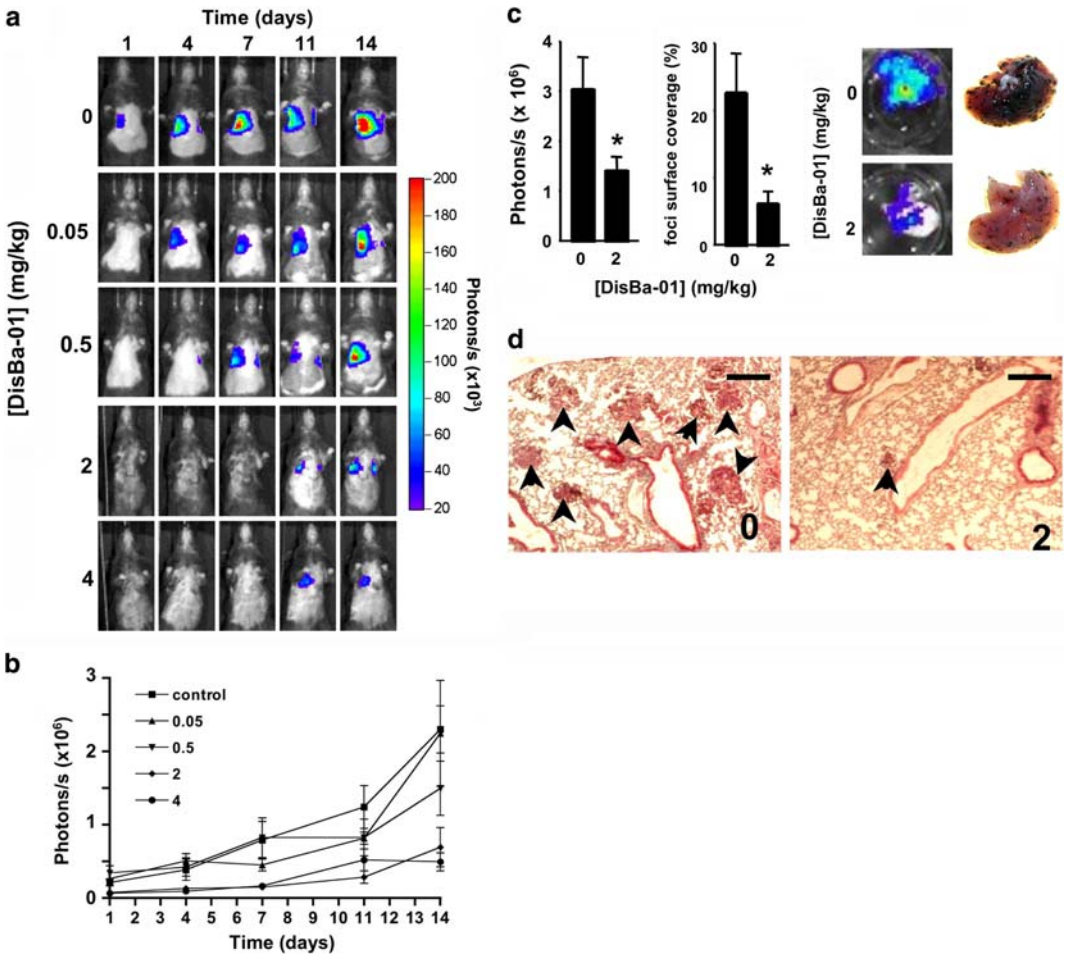

Fig. 7 *Inhibition of lung melanoma metastasis by* Dis*Ba*-01. (**a**) Representative pictures showing the progression of lung melanoma metastasis for each experimental condition (3–8 mice per group) at days 1, 4, 7, 11 and 14 following cell inoculation. Photographs of the mice were superimposed with the corresponding light signal, emitted by the melanoma cells upon intraperitoneal injection of the D-luciferin substrate (150 mg/kg), and represented with a colored scale. (**b**) Quantitative representation of the light signal (in photon per second) produced by the B16F10-2B8 melanoma metastasized in the lungs. (**c**) Ex vivo measurement of light emission and image analyses of pigmented area foci performed at day 14 on excised lung confirmed the in vivo data (left part) (n = 10). In the examples presented (0 or 2 mg/kg of Dis*Ba*-01), the BLI signal correlated with the surface of the lung covered by the pigmented melanoma foci (right part). (**d**) Histological analyses of 5 µm sections of the lung stained with Hematoxylin-Eosin at day 14 confirmed the lower number of micrometastases (arrow heads) formed deep inside the lung tissues when melanoma cells were co-injected with 2 mg/kg of Dis*Ba*-01. Black bars represent 100 µm length. Asterisk indicates a P value <0.001 determined using a Mann–Whitney test

[33]. Accordingly, we observed that B16F10 cell adhesion to immobilized Dis*Ba*-01 was abrogated in the presence of 3 mM EDTA (not shown).

Integrin $\alpha_v\beta_3$ expressed on the surface of activated endothelial cells and tumor cells plays a critical role in tumor angiogenesis and metastasis by regulating adhesive interactions [3–7, 34–39]. In various animal models, the blockade of $\alpha_v\beta_3$ with antibodies or RGD peptides inhibits blood vessel formation without alteration of the pre-existing blood vessels. On the other hand inhibition of blood vessel maturation by $\alpha_v\beta_3$ antagonists causes a regression of tumor angiogenesis and established tumors [40]. $\alpha_v\beta_3$ cooperates with the bFGF receptor to promote events inducing the angiogenic phenotype; it facilitates the survival of stimulated endothelial cells and is specifically required for endothelial migration and adhesion in the presence of bFGF [41, 42]. We showed here that Dis*Ba*-01 inhibits the in vitro adhesion and proliferation of HMEC-1 and the in vivo bFGF-dependent angiogenesis in Matrigel plug. All together, these results suggest that Dis*Ba*-01 can reduce angiogenesis by suppressing $\alpha_v\beta_3$-mediated cell adhesion to ECM proteins of the basement membrane, including vitronectin.

We observed that Dis*Ba*-01 strongly and dose-dependently inhibited the B16F10 melanoma cell adhesion and transiently inhibited their proliferation onto vitronectin. No

potentiation of apoptosis by Dis*Ba*-01 on B16F10 cells in suspension was detected (data not shown). These results strongly suggest that Dis*Ba*-01 is capable of compromising melanoma cell viability by disrupting $\alpha_v\beta_3$ adhesive functions, without direct effect on melanoma cell survival. Noteworthily, the IC_{50} values measured during inhibition of HMEC-1 and B16F10 cells adhesion to vitronectin by Dis*Ba*-01 were comparable to the K_D of the $\alpha_v\beta_3$-Dis*Ba*-01 interaction measured by surface plasmon resonance suggesting that Dis*Ba*-01 and vitronectin interact with similar binding sites on the integrin.

Using a BLI model of mouse lung colonization by luciferase-expressing B16F10 cells, we demonstrated the strong anti-metastatic effect of Dis*Ba*-01 co-injected with the cells. The model that we used bypasses the first steps of spontaneous metastasis such as tumor cell release from the primary tumor, but it involves the hematogeneous dissemination process during which tumor cells interact with circulating platelets and leukocytes and adhere to the vessel wall. Preclinical studies suggest that integrin inhibitors are particularly efficient during this dissemination phase, in contrast to situations where metastases are already established [43, 44]. In fact, we observed by flow cytometry analyses that Dis*Ba*-01 inhibits by up to 40% the in vitro formation of murine platelets-B16F10 cells conjugates (data not shown). However, the administration of Dis*Ba*-01 to mice, 14 days after their injection with melanoma cells, was inefficient to resorb established lung metastases. The inhibitory effect of Dis*Ba*-01 on lung colonization is therefore likely mediated by at least two mechanisms: inhibition of tumor cell adhesion to endothelium and ECM and inhibition of tumor cell-platelet interactions. The in silico model suggests that the other β_3-containing integrin, $\alpha_{IIb}\beta_3$, should also be recognized by Dis*Ba*-01. In support to this, we did observed a strong inhibition of FITC-labelled fibrinogen binding to ADP-activated platelets by DisBa-01 and an anti-platelet aggregation activity of Dis*Ba*-01 both in vitro and in vivo (personal communication [45]). Interestingly, targeting $\alpha_{IIb}\beta_3$ was proven to be efficient to inhibit tumor cell-induced platelet aggregation and metastasis in pre-clinical studies [46].

We did not notice any toxicity of Dis*Ba*-01 for the mouse at the highest dose tested (4 mg/kg). However, we cannot exclude that Dis*Ba*-01 could stimulate the migration of cytotoxic T cells toward the lung micrometastasis to inhibit their development as reported for the RGD-disintegrin Eristostatin [47].

In conclusion, we demonstrated that Dis*Ba*-01, a new recombinant RGD-disintegrin isolated from the venom of *Botrops alternatus* bears potent anti-angiogenic and anti-metastatic activities that are, at least, partly mediated by its interactions with the integrin $\alpha_v\beta_3$. Further studies will be needed to refine the integrin selectivity of Dis*Ba*-01.

Acknowledgments The authors wish to thank Dr Marika Pla and Martine Chopin, Département d'Expérimentation Animale, IFR 105 - Saint Louis-Institut Universitaire d'Hématologie, Paris, France, for their skillful management of animal care facilities, and Monique Etienne from SMBH, Bobigny, France, for histological work. MRC and OHPR were the recipient of research grants provided by FAPESP (Fundação de Amparo à Pesquisa do Estado de São Paulo). This work was supported by travel grants provided in cooperation by INSERM and the Brazilian government (CNPq-INSERM collaboration), a Marie Curie European Reintegration Grant (Project MERG-CT-2004-006377) and grants from the Association pour la Recherche sur le Cancer (Project ARC-7801 and Pôle ARECA) and from the Canceropole Ile-de-France.

References

1. Felding-Habermann B (2003) Integrin adhesion receptors in tumor metastasis. Clin Exp Metastasis 20:203–213
2. Fidler IJ (1975) Biological behavior of malignant melanoma cells correlated to their survival in vivo. Cancer Res 35:218–224
3. Albelda SM, Mette SA, Elder DE et al (1990) Integrin distribution in malignant melanoma: association of the beta 3 subunit with tumor progression. Cancer Res 50:6757–6764
4. Brooks PC, Clark RA, Cheresh DA (1994) Requirement of vascular integrin alpha v beta 3 for angiogenesis. Science 264: 569–571
5. Enenstein J, Waleh NS, Kramer RH (1992) Basic FGF and TGF-beta differentially modulate integrin expression of human microvascular endothelial cells. Exp Cell Res 203:499–503
6. Voura EB, Ramjeesingh RA, Montgomery AM, Siu CH (2001) Involvement of integrin alpha(v)beta(3) and cell adhesion molecule L1 in transendothelial migration of melanoma cells. Mol Biol Cell 12:2699–2710
7. Cooper CR, Chay CH, Pienta KJ (2002) The role of alpha(v)-beta(3) in prostate cancer progression. Neoplasia 4:191–194
8. Hersey P, Sosman J, O'Day S, et al A phase II, randomized, open-label study evaluating the antitumor activity of MEDI-522, a humanized monoclonal antibody directed against the human alpha v beta 3 (avb3) integrin, ± dacarbazine (DTIC) in patients with metastatic melanoma (MM). 2005 ASCO Annual Meeting Proceedings: Journal of Clinical Oncology; 2005
9. Soszka T, Knudsen KA, Beviglia L, Rossi C, Poggi A, Niewiarowski S (1991) Inhibition of murine melanoma cell-matrix adhesion and experimental metastasis by albolabrin, an RGD-containing peptide isolated from the venom of Trimeresurus albolabris. Exp Cell Res 196:6–12
10. Trikha M, De Clerck YA, Markland FS (1994) Contortrostatin, a snake venom disintegrin, inhibits beta 1 integrin-mediated human metastatic melanoma cell adhesion and blocks experimental metastasis. Cancer Res 54:4993–4998
11. Golubkov V, Hawes D, Markland FS (2003) Anti-angiogenic activity of contortrostatin, a disintegrin from Agkistrodon contortrix contortrix snake venom. Angiogenesis 6:213–224
12. Kang IC, Lee YD, Kim DS (1999) A novel disintegrin salmosin inhibits tumor angiogenesis. Cancer Res 59:3754–3760
13. Kim SI, Kim KS, Kim HS et al (2003) Inhibitory effect of the salmosin gene transferred by cationic liposomes on the progression of B16BL6 tumors. Cancer Res 63:6458–6462
14. Yeh CH, Peng HC, Huang TF (1998) Accutin, a new disintegrin, inhibits angiogenesis in vitro and in vivo by acting as integrin alphavbeta3 antagonist and inducing apoptosis. Blood 92: 3268–3276
15. Yeh CH, Peng HC, Yang RS, Huang TF (2001) Rhodostomin, a snake venom disintegrin, inhibits angiogenesis elicited by basic

fibroblast growth factor and suppresses tumor growth by a selective alpha(v)beta(3) blockade of endothelial cells. Mol Pharmacol 59:1333–1342
16. McLane MA, Sanchez EE, Wong A, Paquette-Straub C, Perez JC (2004) Disintegrins. Curr Drug Targets Cardiovasc Haematol Disord 4:327–355
17. Gould RJ, Polokoff MA, Friedman PA et al (1990) Disintegrins: a family of integrin inhibitory proteins from viper venoms. Proc Soc Exp Biol Med 195:168–171
18. Sali A, Blundell TL (1993) Comparative protein modelling by satisfaction of spatial restraints. J Mol Biol 234:779–815
19. Fujii Y, Okuda D, Fujimoto Z, Horii K, Morita T, Mizuno H (2003) Crystal structure of trimestatin, a disintegrin containing a cell adhesion recognition motif RGD. J Mol Biol 332:1115–1122
20. Senn H, Klaus W (1993) The nuclear magnetic resonance solution structure of flavoridin, an antagonist of the platelet GP IIb-IIIa receptor. J Mol Biol 232:907–925
21. Laskowski RA, MacArthur MW, Moss DS, Thornton JM (1993) PROCHECK: a program to check the stereochemical quality of protein structures. J Appl Cryst 26:283–291
22. Bowie JU, Luthy R, Eisenberg D (1991) A method to identify protein sequences that fold into a known three-dimensional structure. Science 253:164–170
23. Vriend G (1990) WHAT IF: a molecular modeling and drug design program. J Mol Graph 8:52–56, 29
24. Lee JO, Rieu P, Arnaout MA, Liddington R (1995) Crystal structure of the A domain from the alpha subunit of integrin CR3 (CD11b/CD18). Cell 80:631–638
25. Xiong JP, Stehle T, Zhang R et al (2002) Crystal structure of the extracellular segment of integrin alpha Vbeta3 in complex with an Arg-Gly-Asp ligand. Science 296:151–155
26. Yahalom D, Wittelsberger A, Mierke DF, Rosenblatt M, Alexander JM, Chorev M (2002) Identification of the principal binding site for RGD-containing ligands in the alpha(V)beta(3) integrin: a photoaffinity cross-linking study. Biochemistry 41: 8321–8331
27. van der Spoel D, Lindahl E, Hess B et al (2005) Gromacs User Manual version 3.3
28. Tsodikov OV, Record MT Jr, Sergeev YV (2002) Novel computer program for fast exact calculation of accessible and molecular surface areas and average surface curvature. J Comput Chem 23:600–609
29. Eliceiri BP, Cheresh DA (1999) The role of alphav integrins during angiogenesis: insights into potential mechanisms of action and clinical development. J Clin Invest 103:1227–1230
30. Takagi J, Kamata T, Meredith J, Puzon-McLaughlin W, Takada Y (1997) Changing ligand specificities of alphavbeta1 and alphavbeta3 integrins by swapping a short diverse sequence of the beta subunit. J Biol Chem 272:19794–19800
31. Ray S, Chattopadhyay N, Biswas N, Chatterjee A (1999) Regulatory molecules in tumor metastasis. J Environ Pathol Toxicol Oncol 18:251–259
32. Monleon D, Esteve V, Kovacs H, Calvete JJ, Celda B (2005) Conformation and concerted dynamics of the integrin-binding site and the C-terminal region of echistatin revealed by homonuclear NMR. Biochem J 387:57–66
33. Baker NA, Sept D, Joseph S, Holst MJ, McCammon JA (2001) Electrostatics of nanosystems: application to microtubules and the ribosome. Proc Natl Acad Sci USA 98:10037–10041
34. Felding-Habermann B, Habermann R, Saldivar E, Ruggeri ZM (1996) Role of beta3 integrins in melanoma cell adhesion to activated platelets under flow. J Biol Chem 271:5892–5900
35. Felding-Habermann B, Mueller BM, Romerdahl CA, Cheresh DA (1992) Involvement of integrin alpha V gene expression in human melanoma tumorigenicity. J Clin Invest 89:2018–2022
36. Hieken TJ, Farolan M, Ronan SG, Shilkaitis A, Wild L, Das Gupta TK (1996) Beta3 integrin expression in melanoma predicts subsequent metastasis. J Surg Res 63:169–173
37. Pilch J, Habermann R, Felding-Habermann B (2002) Unique ability of integrin alpha(v)beta 3 to support tumor cell arrest under dynamic flow conditions. J Biol Chem 277:21930–21938
38. Schneller M, Vuori K, Ruoslahti E (1997) Alphavbeta3 integrin associates with activated insulin and PDGFbeta receptors and potentiates the biological activity of PDGF. EMBO J 16: 5600–5607
39. Sung V, Stubbs JT 3rd, Fisher L, Aaron AD, Thompson EW (1998) Bone sialoprotein supports breast cancer cell adhesion proliferation and migration through differential usage of the alpha(v)beta3 and alpha(v)beta5 integrins. J Cell Physiol 176: 482–494
40. Brooks PC, Montgomery AM, Rosenfeld M et al (1994) Integrin alpha v beta 3 antagonists promote tumor regression by inducing apoptosis of angiogenic blood vessels. Cell 79:1157–1164
41. Dimmeler S, Zeiher AM (2000) Endothelial cell apoptosis in angiogenesis and vessel regression. Circ Res 87:434–439
42. Plopper GE, McNamee HP, Dike LE, Bojanowski K, Ingber DE (1995) Convergence of integrin and growth factor receptor signaling pathways within the focal adhesion complex. Mol Biol Cell 6:1349–1365
43. Harms JF, Welch DR, Samant RS et al (2004) A small molecule antagonist of the alpha(v)beta3 integrin suppresses MDA-MB-435 skeletal metastasis. Clin Exp Metastasis 21:119–128
44. Shannon KE, Keene JL, Settle SL et al (2004) Anti-metastatic properties of RGD-peptidomimetic agents S137 and S247. Clin Exp Metastasis 21:129–138
45. Kauskot A, Cominetti M, Ramos O et al (2007) A novel recombinant RGD-disintegrin from *Bothrops alternatus* (Dis*Ba*-01) antagonizes alphaIIb beta3 and inhibits thrombosis. XXIst Congress of the International Society on Thrombosis and Haemostasis. Blackwell, Geneva
46. Nurden AT, Nurden P (2003) GPIIb/IIIa antagonists and other anti-integrins. Semin Vasc Med 3:123–130
47. McLane MA, Kuchar MA, Brando C, Santoli D, Paquette-Straub CA, Miele ME (2001) New insights on disintegrin-receptor interactions: eristostatin and melanoma cells. Haemostasis 31: 177–182